INTERNATIONAL JOURNAL FOR NUMERICAL METHODS IN FLUIDS
Int. J. Numer. Meth. Fluids 2002; **40**:1145–1162 (DOI: 10.1002/fld.376)

Three-dimensional numerical modelling of free surface flows with non-hydrostatic pressure

Musteyde B. Koçyigit, Roger A. Falconer*,† and Binliang Lin

Cardiff School of Engineering, Cardiff University, Cardiff, U.K.

SUMMARY

A three-dimensional numerical model is developed for incompressible free surface flows. The model is based on the unsteady Reynolds-averaged Navier–Stokes equations with a non-hydrostatic pressure distribution being incorporated in the model. The governing equations are solved in the conventional sigma co-ordinate system, with a semi-implicit time discretization. A fractional step method is used to enable the pressure to be decomposed into its hydrostatic and hydrodynamic components. At every time step one five-diagonal system of equations is solved to compute the water elevations and then the hydrodynamic pressure is determined from a pressure Poisson equation. The model is applied to three examples to simulate unsteady free surface flows where non-hydrostatic pressures have a considerable effect on the velocity field. Emphasis is focused on applying the model to wave problems. Two of the examples are about modelling small amplitude waves where the hydrostatic approximation and long wave theory are not valid. The other example is the wind-induced circulation in a closed basin. The numerical solutions are compared with the available analytical solutions for small amplitude wave theory and very good agreement is obtained. Copyright © 2002 John Wiley & Sons, Ltd.

KEY WORDS: non-hydrostatic pressure distribution; shallow water; sigma co-ordinate; semi-implicit

1. INTRODUCTION

Over the past two decades, two-dimensional and three-dimensional numerical models have been widely used in simulating free surface flows. Although increasing computer power enables three-dimensional models to be more feasible, most of these models are still thought of as being an extension of two-dimensional (depth-integrated) models, and thereby lacking some of the full three-dimensional properties of the flow. In most of these 3D models it is assumed that the vertical acceleration component is small, and hence a hydrostatic pressure distribution is assumed. This assumption is valid for many geophysical applications. However,

* Correspondence to: R. A. Falconer, Cardiff School of Engineering, Cardiff University, P.O. Box 925, Cardiff CF24 OYF, U.K.
† E-mail: falconerra@cardiff.ac.uk

Contract/grant sponsor: Turkish Goverment

Received September 2001
Revised March 2002

in cases such as flows over abruptly changing bed topographies, short wave motion or flows with strong density gradients, the hydrostatic pressure assumption is often no longer valid.

In recent years effort has focused on developing free surface flow models which are free of limitations of the hydrostatic pressure assumption. Some of the models developed are two-dimensional vertical plane models. Typical examples of these models are Stansby and Zhou [1], Zhou and Stansby [2] and Li and Johns [3]. Some researchers such as Gaarthuis [4], Casulli and Stelling [5] and Jankowski [6] have developed three-dimensional numerical models with a non-hydrostatic pressure distribution being included in the model. Casulli and Stelling [5] developed an algorithm in a finite difference implementation, using the idea of fractional step method where the pressure is decomposed into the hydrostatic and the hydrodynamic pressure components, but the effects of the dynamic pressure distribution on the surface elevation were not considered. Gaarthuis [4] computed the non-hydrostatic pressure correction term through an iterative process, which increased the computational cost. Stansby and Zhou [1] developed a model for flows in a two-dimensional vertical plane where they used the finite volume method for discretizing the continuity equation and then solved a Poisson equation for the non-hydrostatic pressure distribution.

The aim of the present study is to develop a 3D numerical model in a sigma co-ordinate system that is efficient in the simulation of free surface flows where the vertical acceleration is not negligible and has an influence on the overall velocity field. The model is tested on three test cases, two of which are the short period waves for which an analytical solution is available and the third one is wind-induced circulation in a closed basin. Due to the lack of analytical solutions and experimental data for 3D problems, the examples involve simulations in the 2D vertical plane, with the model being shown to give accurate and realistic predictions.

2. MATHEMATICAL FORMULATION

The governing three-dimensional equations describing free surface flows in coastal and estuarine waters can be derived from the Navier–Stokes equations. The equations are based on the principle of conservation of the fluid mass and momentum. After Reynolds-averaging of these Navier–Stokes equations, the momentum equations for an incompressible fluid can be expressed in a fully conservative form as

$$\frac{\partial u}{\partial t}+\frac{\partial(uu)}{\partial x}+\frac{\partial(vu)}{\partial y}+\frac{\partial(wu)}{\partial z}=fv-\frac{1}{\rho}\frac{\partial P}{\partial x}+\frac{\partial}{\partial x}\left(\nu_{\mathrm{h}}\frac{\partial u}{\partial x}\right)+\frac{\partial}{\partial y}\left(\nu_{\mathrm{h}}\frac{\partial u}{\partial y}\right)+\frac{\partial}{\partial z}\left(\nu_{\mathrm{v}}\frac{\partial u}{\partial z}\right) \tag{1}$$

$$\frac{\partial v}{\partial t}+\frac{\partial(uv)}{\partial x}+\frac{\partial(vv)}{\partial y}+\frac{\partial(wv)}{\partial z}=-fu-\frac{1}{\rho}\frac{\partial P}{\partial y}+\frac{\partial}{\partial x}\left(\nu_{\mathrm{h}}\frac{\partial v}{\partial x}\right)+\frac{\partial}{\partial y}\left(\nu_{\mathrm{h}}\frac{\partial v}{\partial y}\right)+\frac{\partial}{\partial z}\left(\nu_{\mathrm{v}}\frac{\partial v}{\partial z}\right) \tag{2}$$

$$\frac{\partial w}{\partial t}+\frac{\partial(uw)}{\partial x}+\frac{\partial(vw)}{\partial y}+\frac{\partial(ww)}{\partial z}=-g-\frac{1}{\rho}\frac{\partial P}{\partial z}+\frac{\partial}{\partial x}\left(v_{\mathrm{h}}\frac{\partial w}{\partial x}\right)+\frac{\partial}{\partial y}\left(v_{\mathrm{h}}\frac{\partial w}{\partial y}\right)+\frac{\partial}{\partial z}\left(v_{\mathrm{v}}\frac{\partial w}{\partial z}\right) \tag{3}$$

where x, y, and z are the Cartesian co-ordinates oriented eastward, northward, and upward, respectively; u, v and w are the velocity components in the horizontal x, y and the vertical z-directions; P is the pressure; t is the time; g is the gravitational acceleration; ρ is the fluid density; f is the Coriolis parameter; v_{h} and v_{v} are the kinematic eddy viscosity coefficients in the horizontal and vertical directions, respectively.

The vertical eddy viscosity v_{v} is represented using a two-layer mixing length model [7] written in the form

$$v_{\mathrm{v}}=l_m^2\left[\left(\frac{\partial u}{\partial z}\right)^2+\left(\frac{\partial v}{\partial z}\right)^2\right]^{1/2} \tag{4}$$

where l_{m} is the mixing length defined as

$$\begin{aligned} l_{\mathrm{m}}&=\kappa z \quad \text{for } \kappa z\leqslant 0.1H \\ l_{\mathrm{m}}&=0.1H \quad \text{for } \kappa z>0.1H \end{aligned} \tag{5}$$

where κ is the von Kármán's constant (0.41) and H is the depth of flow.

For the pressure term P, Equations (1)–(3) can be decomposed into the hydrostatic (i.e. $P_{\mathrm{h}}=\rho g(\eta-z)$) and hydrodynamic (i.e. $P_{\mathrm{dyn}}=q$) components, respectively, giving

$$P=P_{\mathrm{h}}+P_{\mathrm{dyn}}=\rho g(\eta-z)+q \tag{6}$$

where η is the water surface above horizontal datum and $z=0$ at the undisturbed water surface.

Substitution of Equation (6) into Equations (1)–(3) therefore yields

$$\frac{\partial u}{\partial t}+\frac{\partial(uu)}{\partial x}+\frac{\partial(vu)}{\partial y}+\frac{\partial(wu)}{\partial z}=fv-g\frac{\partial \eta}{\partial x}-\frac{1}{\rho}\frac{\partial q}{\partial x}+\frac{\partial}{\partial x}\left(v_{\mathrm{h}}\frac{\partial u}{\partial x}\right)+\frac{\partial}{\partial y}\left(v_{\mathrm{h}}\frac{\partial u}{\partial y}\right)+\frac{\partial}{\partial z}\left(v_{\mathrm{v}}\frac{\partial u}{\partial z}\right) \tag{7}$$

$$\frac{\partial v}{\partial t}+\frac{\partial(uv)}{\partial x}+\frac{\partial(vv)}{\partial y}+\frac{\partial(wv)}{\partial z}=-fu-g\frac{\partial \eta}{\partial y}-\frac{1}{\rho}\frac{\partial q}{\partial y}+\frac{\partial}{\partial x}\left(v_{\mathrm{h}}\frac{\partial v}{\partial x}\right)+\frac{\partial}{\partial y}\left(v_{\mathrm{h}}\frac{\partial v}{\partial y}\right)+\frac{\partial}{\partial z}\left(v_{\mathrm{v}}\frac{\partial v}{\partial z}\right) \tag{8}$$

$$\frac{\partial w}{\partial t}+\frac{\partial (uw)}{\partial x}+\frac{\partial (vw)}{\partial y}+\frac{\partial (ww)}{\partial z}$$
$$=-\frac{1}{\rho}\frac{\partial q}{\partial z}+\frac{\partial}{\partial x}\left(v_{\mathrm{h}}\frac{\partial w}{\partial x}\right)+\frac{\partial}{\partial y}\left(v_{\mathrm{h}}\frac{\partial w}{\partial y}\right)+\frac{\partial}{\partial z}\left(v_{\mathrm{v}}\frac{\partial w}{\partial z}\right) \tag{9}$$

Likewise, the conservation of mass may be expressed through the continuity equation, giving

$$\frac{\partial u}{\partial x}+\frac{\partial v}{\partial y}+\frac{\partial w}{\partial z}=0 \tag{10}$$

By integrating the continuity equation (10) over the depth and applying the kinematic boundary condition at the free surface, the well-known free surface equation can be written as

$$\frac{\partial \eta}{\partial t}+\frac{\partial}{\partial x}\int_{-h}^{\eta} u\,\mathrm{d}z+\frac{\partial}{\partial y}\int_{-h}^{\eta} v\,\mathrm{d}z=0 \tag{11}$$

To define the bed and surface boundaries accurately, the sigma co-ordinate system is used in the vertical direction. The numerical mesh thus fits the free surface and bed very closely enabling a higher resolution near these boundaries where sharp velocity gradients may be observed. The transformation between the Cartesian co-ordinate system and the sigma co-ordinate system is given as

$$\sigma=\frac{z-\eta(x,y,t)}{h(x,y)+\eta(x,y,t)}=\frac{z-\eta(x,y,t)}{H(x,y,t)} \tag{12}$$

where σ is the transformed vertical co-ordinate, z is the arbitrary distance along the vertical axis, $\eta(x,y,t)$ is the water surface elevation above datum, $h(x,y)$ is the elevation of the bed below datum and H is the total depth of the water column.

Thus, the governing Equations (1)–(3) in sigma co-ordinates may be written in a conservative form as

$$\frac{\partial (Hu)}{\partial t}+\frac{\partial (Huu)}{\partial x}+\frac{\partial (Hvu)}{\partial y}+\frac{\partial (\omega u)}{\partial \sigma}$$
$$=fHv-Hg\frac{\partial \eta}{\partial x}-\frac{H}{\rho}\frac{\partial q}{\partial x}+H\frac{\partial}{\partial x}\left(v_{\mathrm{h}}\frac{\partial u}{\partial x}\right)+H\frac{\partial}{\partial y}\left(v_{\mathrm{h}}\frac{\partial u}{\partial y}\right)+\frac{\partial}{\partial \sigma}\left(\frac{v_{\mathrm{v}}}{H}\frac{\partial u}{\partial \sigma}\right) \tag{13}$$

$$\frac{\partial (Hv)}{\partial t}+\frac{\partial (Hvu)}{\partial x}+\frac{\partial (Hvv)}{\partial y}+\frac{\partial (\omega v)}{\partial \sigma}$$
$$=-fHu-Hg\frac{\partial \eta}{\partial y}-\frac{H}{\rho}\frac{\partial q}{\partial y}+H\frac{\partial}{\partial x}\left(v_{\mathrm{h}}\frac{\partial v}{\partial x}\right)+H\frac{\partial}{\partial y}\left(v_{\mathrm{h}}\frac{\partial v}{\partial y}\right)+\frac{\partial}{\partial \sigma}\left(\frac{v_{\mathrm{v}}}{H}\frac{\partial v}{\partial \sigma}\right) \tag{14}$$

$$\frac{\partial(Hw)}{\partial t}+\frac{\partial(Hwu)}{\partial x}+\frac{\partial(Hwv)}{\partial y}+\frac{\partial(w\omega)}{\partial\sigma}$$
$$=-\frac{1}{\rho}\frac{\partial q}{\partial\sigma}+H\frac{\partial}{\partial x}\left(v_{\mathrm{h}}\frac{\partial w}{\partial x}\right)+H\frac{\partial}{\partial y}\left(v_{\mathrm{h}}\frac{\partial w}{\partial y}\right)+\frac{\partial}{\partial\sigma}\left(\frac{v_{\mathrm{v}}}{H}\frac{\partial w}{\partial\sigma}\right) \tag{15}$$

where a new vertical velocity ω, defined as $\omega=H(\mathrm{d}\sigma/\mathrm{d}t)$, is related to w by the following relationship:

$$\omega=w-u\left(\sigma\frac{\partial H}{\partial x}+\frac{\partial\eta}{\partial x}\right)-v\left(\sigma\frac{\partial H}{\partial y}+\frac{\partial\eta}{\partial y}\right)-\left(\sigma\frac{\partial H}{\partial t}+\frac{\partial\eta}{\partial t}\right) \tag{16}$$

The horizontal gradients of the non-hydrostatic pressure q and the horizontal diffusion terms in Equations (13)–(15) are not transformed into the sigma co-ordinate system to avoid large errors, especially near steep bottom slopes where small pressure gradients might be the result of the sum of two relatively large terms of opposite sign, resulting in a relatively large error in the pressure gradient that can induce artificial flows [8, 9].

3. NUMERICAL DISCRETIZATION AND SOLUTION METHOD

A fractional step method is used to solve the three-dimensional free surface flow equations in two steps. For the first step the gradient of the surface elevation in the horizontal momentum Equations (13) and (14) and the horizontal velocities in the surface Equation (11) are discretized using the θ-method. In the momentum equations, the vertical viscosity terms are dicretized implicitly for stability, while the rest of the terms, i.e. the advection, Coriolis and horizontal viscosity terms, are discretized explicitly. The non-hydrostatic pressure is also included in the momentum equations for incorporating the effects of the hydrodynamic pressure distribution on the free-surface elevation.

For the discretization of the equations, the conventional staggered mesh system is used as shown in Figure 1. The centre of the cells is numbered with indices i,j,k, where $i=1,\ldots,I, j=1,\ldots,J$ and $k=1,\ldots,K$, with $k=1$ for the surface cell and $k=K$ for the bed cell. The u-velocity is then defined at $i+\frac{1}{2},j,k$; the velocity v is defined at $i,j+\frac{1}{2},k$ and the vertical

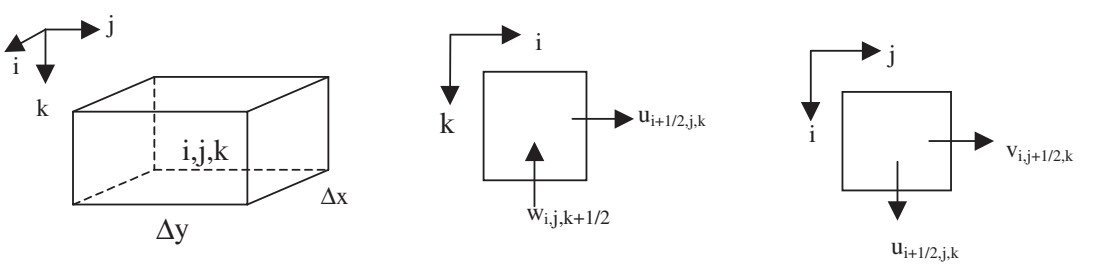

Figure 1. Staggered grid mesh system.

velocities w and ω are defined at the node $i,j,k-\frac{1}{2}$. The surface elevation η is defined at the cell centre (i,j) and the water depth $H(x,y)$ is specified at the centre of each grid side, i.e. $i+\frac{1}{2},j$ and $i,j+\frac{1}{2}$, thereby providing a comprehensive representation of the bathymetry. Finally, the hydrodynamic pressure term q is defined at the node i,j,k. σ represents the sigma value of a level and $\Delta\sigma$ is the vertical mesh spacing in sigma co-ordinates.

The first term in the form of $\partial(H\phi)/\partial t$ on the left-hand side of Equations (13)–(15) can conveniently be expanded to give

$$\frac{\partial(H\phi)}{\partial t} = H\frac{\partial\phi}{\partial t} + \phi\frac{\partial H}{\partial t} \tag{17}$$

where ϕ stands for u,v,w, respectively. The discretization of the momentum Equations (13) and (14) then takes the form

$$\tilde{u}^{n+1}_{i+1/2,j,k} = Fu^{n}_{i+1/2,j,k} - g\frac{\Delta t}{\Delta x}[\theta(\eta^{n+1}_{i+1,j}-\eta^{n+1}_{i,j}) + (1-\theta)(\eta^{n}_{i+1,j}-\eta^{n}_{i,j})] + \frac{1}{H^{n}_{i+1/2,j}\Delta\sigma_k}$$
$$\times\left[v_{k-1/2}\frac{\tilde{u}^{n+1}_{i+1/2,j,k-1}-\tilde{u}^{n+1}_{i+1/2,j,k}}{H^{n}_{i+1/2,j}\Delta\sigma_{k-1/2}} - v_{k+1/2}\frac{\tilde{u}^{n+1}_{i+1/2,j,k}-\tilde{u}^{n+1}_{i+1/2,j,k+1}}{H^{n}_{i+1/2,j}\Delta\sigma_{k+1/2}}\right] \tag{18}$$

$$\tilde{v}^{n+1}_{i,j+1/2,k} = Fv^{n}_{i,j+1/2,k} - g\frac{\Delta t}{\Delta y}[\theta(\eta^{n+1}_{i,j+1}-\eta^{n+1}_{i,j}) + (1-\theta)(\eta^{n}_{i,j+1}-\eta^{n}_{i,j})] + \frac{1}{H^{n}_{i,j+1/2}\Delta\sigma_k}$$
$$\times\left[v_{k-1/2}\frac{\tilde{v}^{n+1}_{i,j+1/2,k-1}-\tilde{v}^{n+1}_{i,j+1/2,k}}{H^{n}_{i,j+1/2}\Delta\sigma_{k-1/2}} - v_{k+1/2}\frac{\tilde{v}^{n+1}_{i,j+1/2,k}-\tilde{v}^{n+1}_{i,j+1/2,k+1}}{H^{n}_{i,j+1/2}\Delta\sigma_{k+1/2}}\right] \tag{19}$$

$$\tilde{w}^{n+1}_{i,j,k-1/2} = Fw^{n}_{i,j,k-1/2} + \frac{1}{H^{n}_{i,j}\Delta\sigma_{k-1/2}}\left[v_{k-1}\frac{\tilde{w}^{n+1}_{i,j,k-1}-\tilde{w}^{n+1}_{i,j,k}}{H^{n}_{i,j}\Delta\sigma_{k-1}} - v_k\frac{\tilde{w}^{n+1}_{i,j,k}-\tilde{w}^{n+1}_{i,j,k+1}}{H^{n}_{i,j}\Delta\sigma_k}\right] \tag{20}$$

where $\Delta\sigma_k = \sigma_{k+1}-\sigma_k$ is the vertical mesh spacing (i.e. distance between two consecutive level surfaces), n is the current time level, $n+1$ is the new time level and Δt is the time step. F is a finite difference operator that includes the explicit discretization of the advective terms, the horizontal viscosity and the Coriolis acceleration. The operator F also includes the non-hydrostatic pressure term q at the time step n. Equations (18) and (19) can now be written in a matrix form giving

$$\mathbf{A}^{n}_{i+1/2,j}\tilde{\mathbf{U}}^{n+1}_{i+1/2,j} = G^{n}_{i+1/2,j} - \theta g\frac{\Delta t}{\Delta x}(\eta^{n+1}_{i+1,j}-\eta^{n+1}_{i,j})\Delta\sigma^{n}_{i+1/2,j} \tag{21}$$

$$\mathbf{A}^{n}_{i,j+1/2}\tilde{\mathbf{V}}^{n+1}_{i,j+1/2} = G^{n}_{i,j+1/2} - \theta g\frac{\Delta t}{\Delta y}(\eta^{n+1}_{i,j+1}-\eta^{n+1}_{i,j})\Delta\sigma^{n}_{i,j+1/2} \tag{22}$$

Details of the matrix in the x-direction are given in Appendix A.

In order to determine $\eta_{i,j}^{n+1}$, and for numerical stability, the new intermediate velocity field must satisfy each grid cell i,j of the finite volume representation of the free surface equation. Hence, the free surface Equation (11) can be discretized and written in matrix notation giving

$$\eta_{i,j}^{n+1} = \delta_{i,j}^{n} - \theta\frac{\Delta t}{\Delta x}[(\Delta\sigma_{i+1/2,j}^{n})^{\mathrm{T}}\tilde{U}_{i+1/2,j}^{n+1} - (\Delta\sigma_{i-1/2,j}^{n})^{\mathrm{T}}\tilde{U}_{i=1/2,j}^{n+1}]$$

$$- \theta\frac{\Delta t}{\Delta y}[(\Delta\sigma_{i,j+1/2}^{n})^{\mathrm{T}}\tilde{V}_{i,j+1/2}^{n+1} - (\Delta\sigma_{i,j-1/2}^{n})^{\mathrm{T}}\tilde{V}_{i,j-1/2}^{n+1}] \tag{23}$$

where $\tilde{\mathbf{U}}_{i+1/2,j}^{n+1}$ and $\tilde{\mathbf{V}}_{i,j+1/2}^{n+1}$ = vectors of u and v at the specified horizontal locations. $\delta_{i,j}^{n}$ contains all of the explicit terms in Equation (23) giving

$$\delta_{i,j}^{n+1} = \eta_{i,j}^{n} - (1-\theta)\frac{\Delta t}{\Delta x}\left[\sum_{k=1}^{k=K}\Delta\sigma_{i+1/2,j,k}^{n}u_{i+1/2,j,k}^{n} - \sum_{k=1}^{k=K}\Delta\sigma_{i-1/2,j,k}^{n}u_{i-1/2,j,k}^{n}\right]$$

$$- (1-\theta)\frac{\Delta t}{\Delta y}\left[\sum_{k=1}^{k=K}\Delta\sigma_{i,j+1/2,k}^{n}v_{i,j+1/2,k}^{n} - \sum_{k=1}^{k=K}\Delta\sigma_{i,j-1/2,k}^{n}v_{i,j-1/2,k}^{n}\right] \tag{24}$$

Substitution of the expressions for $\tilde{\mathbf{U}}_{i+1/2,j}^{n+1}$ and $\tilde{\mathbf{V}}_{i,j+1/2}^{n+1}$ from Equations (21) and (22) into Equation (23) yields

$$\eta_{i,j}^{n+1} - g\theta^2\frac{\Delta t^2}{\Delta x^2}\{[(\Delta\sigma)^{\mathrm{T}}\mathbf{A}^{-1}\Delta\sigma]_{i+1/2,j}^{n}(\eta_{i+1,j}^{n+1} - \eta_{i,j}^{n+1}) - [(\Delta\sigma)^{\mathrm{T}}\mathbf{A}^{-1}\Delta\sigma]_{i-1/2,j}^{n}(\eta_{i,j}^{n+1} - \eta_{i-1,j}^{n+1})\}$$

$$- g\theta^2\frac{\Delta t^2}{\Delta y^2}\{[(\Delta\sigma)^{\mathrm{T}}\mathbf{A}^{-1}\Delta\sigma]_{i,+1/2}^{n}(\eta_{i,j+1}^{n+1} - \eta_{i,j}^{n+1}) - [(\Delta\sigma)^{\mathrm{T}}\mathbf{A}^{-1}\Delta\sigma]_{i,j-1/2}^{n}(\eta_{i,j}^{n+1} - \eta_{i,j-1}^{n+1})\}$$

$$= \delta_{i,j}^{n} - \frac{\Delta t}{\Delta x}\{[(\Delta\sigma)^{\mathrm{T}}\mathbf{A}^{-1}\mathbf{G}]_{i+1/2,j}^{n} - [(\Delta\sigma)^{\mathrm{T}}\mathbf{A}^{-1}\mathbf{G}]_{i-1/2,j}^{n}\}$$

$$- \frac{\Delta t}{\Delta y}\{[(\Delta\sigma)^{\mathrm{T}}\mathbf{A}^{-1}\mathbf{G}]_{i,j+1/2}^{n} - [(\Delta\sigma)^{\mathrm{T}}\mathbf{A}^{-1}\mathbf{G}]_{i,j-1/2}^{n}\} \tag{25}$$

This five-diagonal system of equations, with the unknowns $\tilde{u}_{i+1/2,j,k}^{n+1}$, $\tilde{v}_{i,j+1/2,k}^{n+1}$ and $\eta_{i,j}^{n+1}$ being specified over the entire computational mesh, has to be solved at each time step to determine recursively values of the field variables. Once the new surface elevation is determined, Equations (21) and (22) are solved to determine the horizontal velocity field. With the help of a flag introduced in the code, the model can be run with or without the hydrostatic approximation. If the model is run without the hydrostatic assumption, then the vertical momentum Equation (18) is used to determine the intermediate vertical velocity. Otherwise, the vertical velocities w and ω at the new time

level $n+1$ are to be found from the continuity Equation (10) and Equation (16), respectively.

In the second step the new velocity fields $u^{n+1}_{i+1/2,j,k}$, $v^{n+1}_{i,j+1/2,k}$ and $w^{n+1}_{i,j,k+1/2}$ are computed by correcting the intermediate velocity field ($\tilde{u}^{n+1}_{i+1/2,j,k}$, $\tilde{v}^{n+1}_{i,j+1/2,k}$ and $\tilde{w}^{n+1}_{i,j,k+1/2}$) with the gradient of the hydrodynamic pressure correction term, since the intermediate velocity field will not satisfy the local continuity equation. Hence, the hydrodynamic pressure correction term is determined by requiring that the new velocity field is convergent. If the correction term for the non-hydrostatic pressure is q', then the corrected value is given by

$$q = q^* + q' \tag{26}$$

where q^* is the uncorrected hydrodynamic pressure and q' is the hydrodynamic pressure correction term. The discrete momentum equations therefore become

$$u^{n+1}_{i+1/2,j,k} = \tilde{u}^{n+1}_{i+1/2,j,k} - \frac{\Delta t}{\Delta x}(q'^{n+1}_{i+1,j,k} - q'^{n+1}_{i,j,k}) \tag{27}$$

$$v^{n+1}_{i,j+1/2,k} = \tilde{v}^{n+1}_{i,j+1/2,k} - \frac{\Delta t}{\Delta y}(q'^{n+1}_{i,j+1,k} - q'^{n+1}_{i,j,k}) \tag{28}$$

$$w^{n+1}_{i,j,k+1/2} = \tilde{w}^{n+1}_{i,j,k+1/2} - \frac{\Delta t}{H^n_{i,j}\Delta\sigma_{k+1/2}}(q'^{n+1}_{i,j,k} - q'^{n+1}_{i,j,k+1}) \tag{29}$$

In each computational grid the incompressibility condition should be satisfied. The discretized incompressibility condition can be discretized as

$$\frac{H^{n+1}_{i+1/2,j}u^{n+1}_{i+1/2,j,k} - H^{n+1}_{i-1/2,j}u^{n+1}_{i-1/2,j,k}}{\Delta x} + \frac{H^{n+1}_{i,j+1/2}v^{n+1}_{i,j+1/2,k} - H^{n+1}_{i,j-1/2}v^{n+1}_{i,j-1/2,k}}{\Delta y} + \frac{w^{n+1}_{i,j,k-1/2} - w^{n+1}_{i,j,k+1/2}}{\Delta z} = 0 \tag{30}$$

The expressions for the new velocities from Equations (27)–(29) are substituted into the incompressibility Equation (30), resulting in the following finite difference Poisson equation for the hydrodynamic pressure correction term

$$\frac{\Delta t}{\Delta x^2}\Delta\sigma^n_{i+1/2,j,k}(q'^{n+1}_{i+1,j,k} - q'^{n+1}_{i,j,k}) - \frac{\Delta t}{\Delta x^2}\Delta\sigma^n_{i+1/2,j,k}(q'^{n+1}_{i,j,k} - q'^{n+1}_{i-1,j,k}) + \frac{\Delta t}{\Delta y^2}\Delta\sigma^n_{i,j+1/2,k}(q'^{n+1}_{i,j+1,k} - q'^{n+1}_{i,j,k}) - \frac{\Delta t}{\Delta y^2}\Delta\sigma^n_{i,j+1/2,k}(q'^{n+1}_{i,j,k} - q'^{n+1}_{i,j-1,k}) + \frac{1}{\Delta\sigma^n_{i,j,k-1/2}}(q'^{n+1}_{i,j,k-1} - q'^{n+1}_{i,j,k}) - \frac{1}{\Delta\sigma^n_{i,j,k+1/2}}(q^{n+1}_{i,j,k} - q'^{n+1}_{i,j,k+1})$$

$$= \frac{1}{\Delta x}[\Delta\sigma^n_{i+1/2,j,k}\tilde{u}^{n+1}_{i+1/2,j,k} - \Delta\sigma^n_{i-1/2,j,k}\tilde{u}^{n+1}_{i-1/2,j,k}] + \frac{1}{\Delta y}[\Delta\sigma^n_{i,j+1/2,k}\tilde{v}^{n+1}_{i,j+1/2,k}$$

$$-\Delta\sigma^n_{i,j-1/2,k}\tilde{v}^{n+1}_{i,j-1/2,k}] + [\tilde{w}^{n+1}_{i,j,k-1/2} - \tilde{w}^{n+1}_{i,j,k+1/2}] \tag{31}$$

Thus, Equation (31) forms a seven diagonal linear system and can be solved iteratively by the conjugate gradient method. Once the hydrodynamic pressure correction term is computed, the final velocity field at the new time level can be determined from Equations (27) to (29) and the hydrodynamic pressure field is updated with the hydrodynamic pressure correction term.

The system of equations are subject to various types of boundary conditions. At the solid impermeable boundaries, no mass flux is allowed through the boundary and therefore zero normal flow is imposed in Equations (27)–(29). For the pressure Poisson Equation (31), a Neumann type of boundary condition is used. At the surface, the hydrodynamic pressure q is set to zero, so a Dirichlet type of boundary condition is specified in Equation (31). For the case of a wind stress on the surface, the shear stress at the free surface is given by

$$\rho\nu_v\frac{\partial u}{\partial z} = \tau^w_{xz}, \quad \rho\nu_v\frac{\partial v}{\partial z} = \tau^w_{yz} \tag{32a,b}$$

where τ^w_{xz} and τ^w_{yz} are the components of the wind stress in the x- and y-direction, respectively. At the bed a logarithmic velocity profile within the bottom layer is assumed and the following equations are obtained for the bed shear stress:

$$\nu\frac{\partial u}{\partial z} = \frac{\tau^b_{xz}}{\rho} = \frac{\sqrt{(u^n_{i+1/2,j,K})^2 + (v^n_{i,j+1/2,K})^2}}{\left[2.5\ln\left(\frac{30d}{2.72k_s}\right)\right]^2}u^{n+1}_{i+1/2,j,K} \tag{33a}$$

$$\nu\frac{\partial v}{\partial z} = \frac{\tau^b_{yz}}{\rho} = \frac{\sqrt{(u^n_{i+1/2,j,K})^2 + (v^n_{i,j+1/2,K})^2}}{\left[2.5\ln\left(\frac{30d}{2.72k_s}\right)\right]^2}v^{n+1}_{i,j+1/2,K} \tag{33b}$$

where τ^b_{xz} and τ^b_{yz} are the components of bed shear stress in x- and y-direction, d is the thickness of the bottom layer, and k_s is the roughness length.

At the free surface $q = 0$ and w is determined in a surface cell by applying the continuity Equation (10). At the bed, the impermeability condition is applied, wherein $w^{n+1}_{i,j,K+1/2} = 0$.

Since the θ-method is used in the model, it is important to decide the value of θ to be used in the numerical model. When $\theta = 1$, the algorithm becomes fully implicit and wave damping problems may arise. To avoid wave damping and have high accuracy and efficiency, a semi-implicit scheme is used where $\theta = \frac{1}{2}$ so that the average values of the pressure gradient and the velocities are used in the momentum equations and free surface equation.

4. MODEL APPLICATIONS

A very good example for testing mass and energy conservation, and demonstrating the effects of the hydrodynamic pressure on the circulation pattern, is the small amplitude wave test case. First, a uni-nodal standing wave is simulated. For this test, an inviscid fluid of constant density is confined in a closed basin with a square base of length $L = 10$ m and with an equilibrium depth of $H = 10$ m. The square basin is discretized with 400 square cells of sides $\Delta x = \Delta z = 0.5$ m. A zero initial velocity is assumed and the initial free surface elevation is given by

$$\eta(x) = A\cos(kx), \quad 0 < x < L \tag{34}$$

where A is the wave amplitude, $k = 2\pi/nL$ and $n = 2$ for a uni-nodal wave. The amplitude of the wave is taken to be 0.1 m, 1% of the water depth so that small amplitude wave theory applies. Applying small amplitude wave theory, the celerity of the wave is computed according to the relationship

$$c = [(g/k)\tanh(kH)]^{1/2} \tag{35}$$

where c is the wave celerity.

Details of small amplitude wave theory and the analytical solutions can be found in Reference [6]. In the numerical simulation of small amplitude waves, the wave celerity and the period of oscillation are calculated as 3.64 m/s and 3.586 s, respectively. A small time step

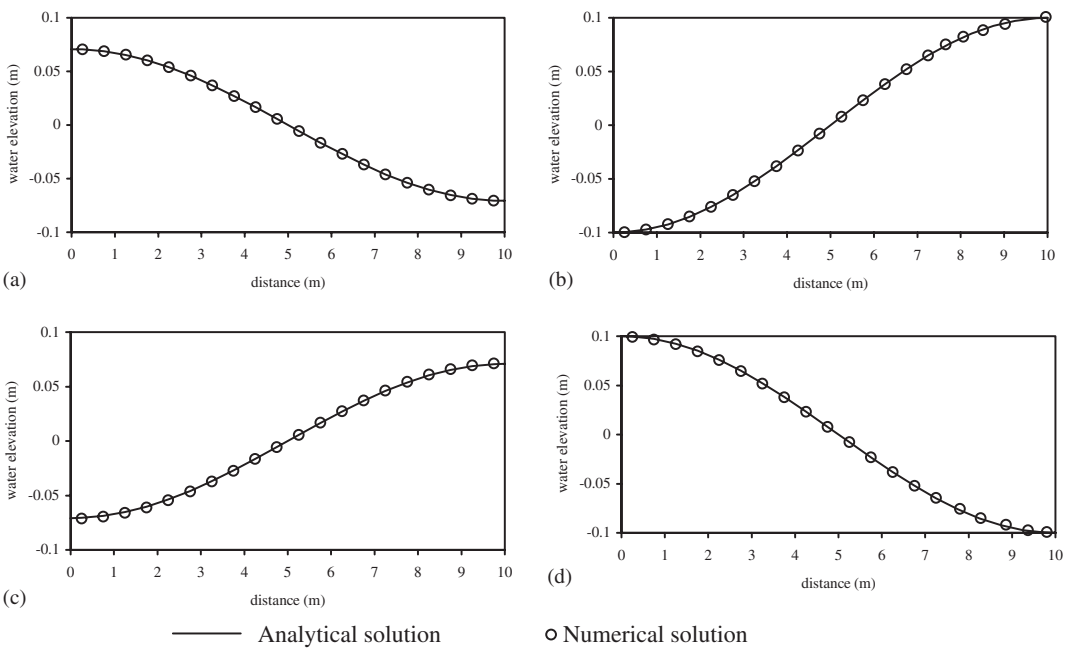

Figure 2. Comparison of water elevation with numerical and analytical solutions for: (a) $T/8$; (b) $T/2$; (c) $5T/8$; and (d) $2T$.

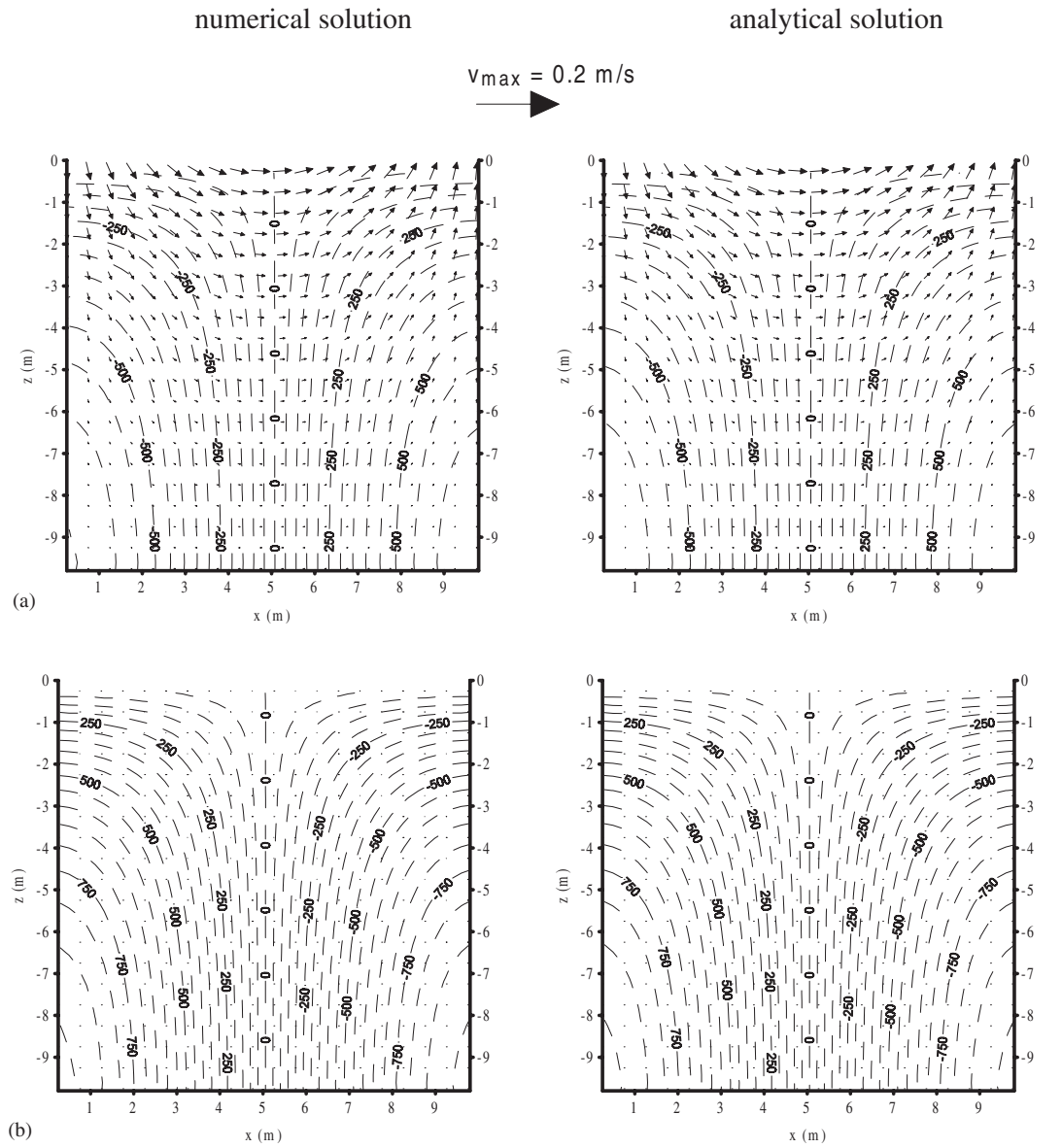

Figure 3. Comparison between numerical and analytical solutions of velocity and hydrodynamic pressure fields in the vertical section for: (a) $t = T/8$; (b) $t = T/2$; (c) $t = 5T/8$; and (d) $t = 2T$. Iso-lines of dynamic pressure are shown at intervals of 50 Pa.

of $\Delta t = 0.0001$ s is used for higher accuracy. At the free surface a zero Neumann boundary condition is applied for all three velocity components, while at wall boundaries the impermeability or free slip condition is applied. The hydrodynamic pressure is set to zero at the surface and an impermeability boundary condition is imposed at all wall boundaries.

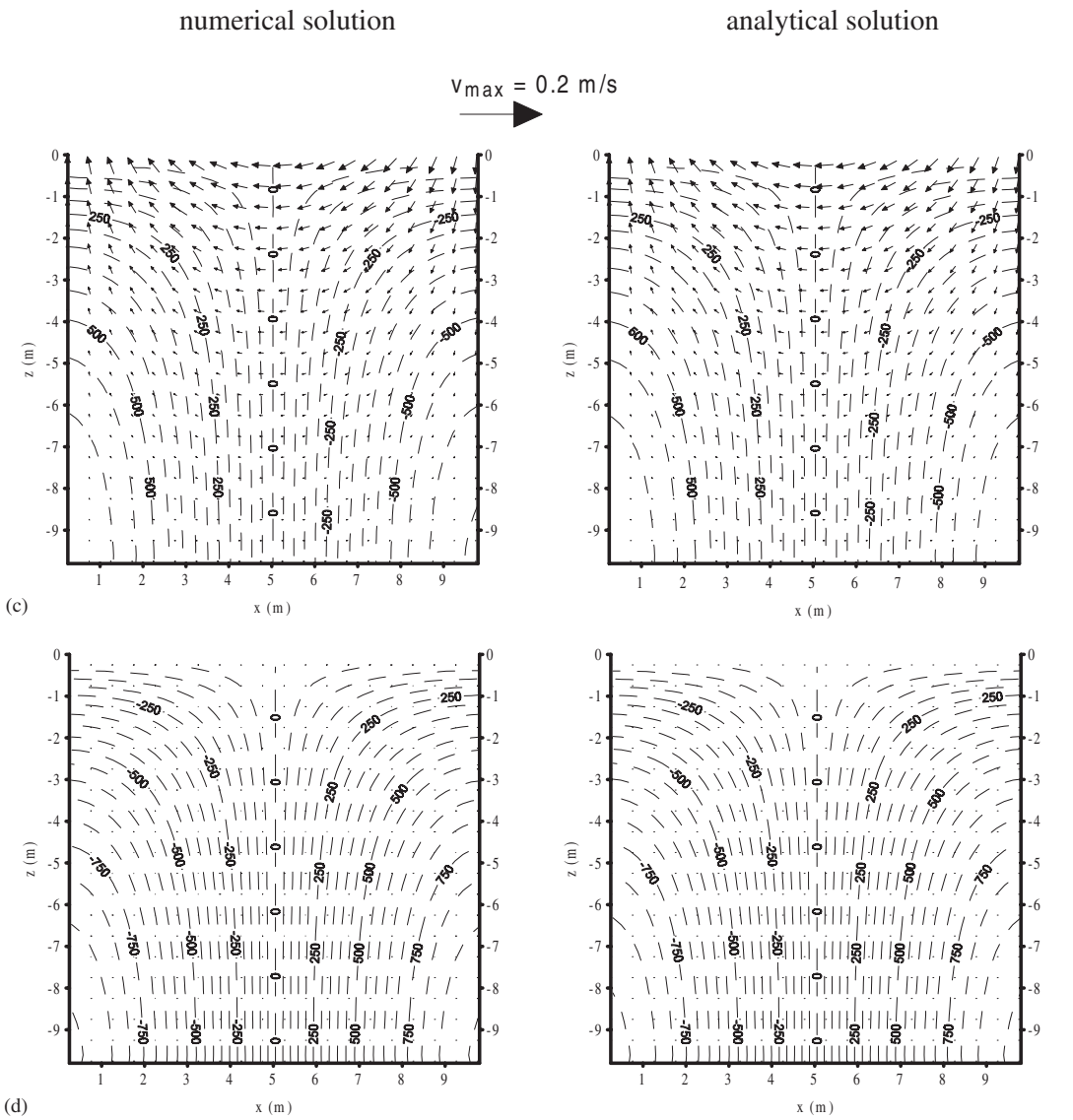

Figure 3. (*Continued*).

Comparisons of the free surface elevations obtained from the analytical solution and numerical model predictions are given in Figure 2 for the phases $T/8$, $T/2$, $5T/8$ and $2T$. As can be seen from the results, there is very good agreement between the numerical results and the analytical solution for short period waves. Comparisons of the numerical model predictions and analytical solutions for the velocities and hydrodynamic pressure distributions in the vertical section of the basin are shown in Figure 3 for the same phases of motion. The comparison of velocity and pressure field also shows very good agreement between the analytical solutions

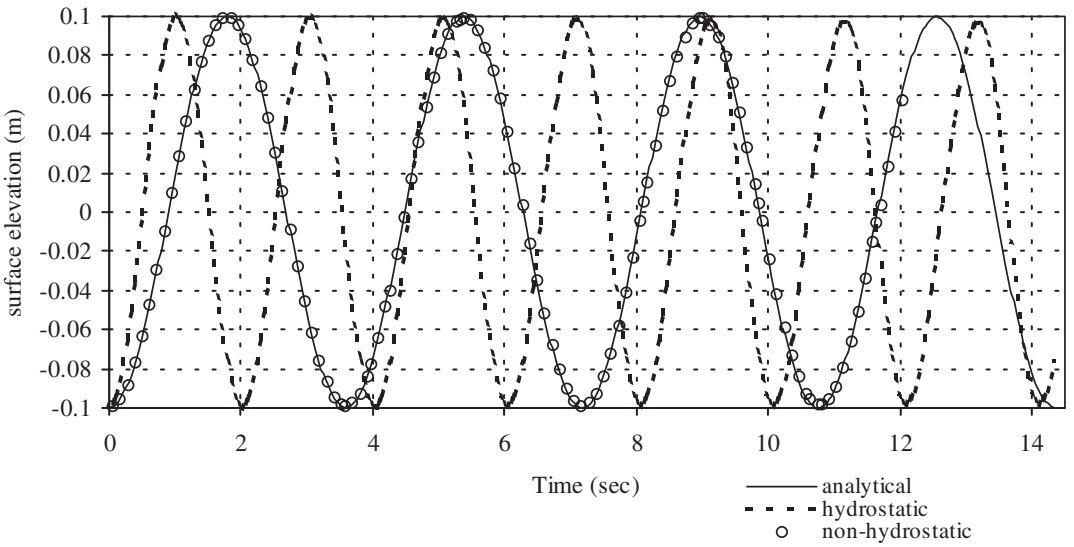

Figure 4. Comparison of analytical and numerical solutions, both with and without hydrostatic assumption for small amplitude wave.

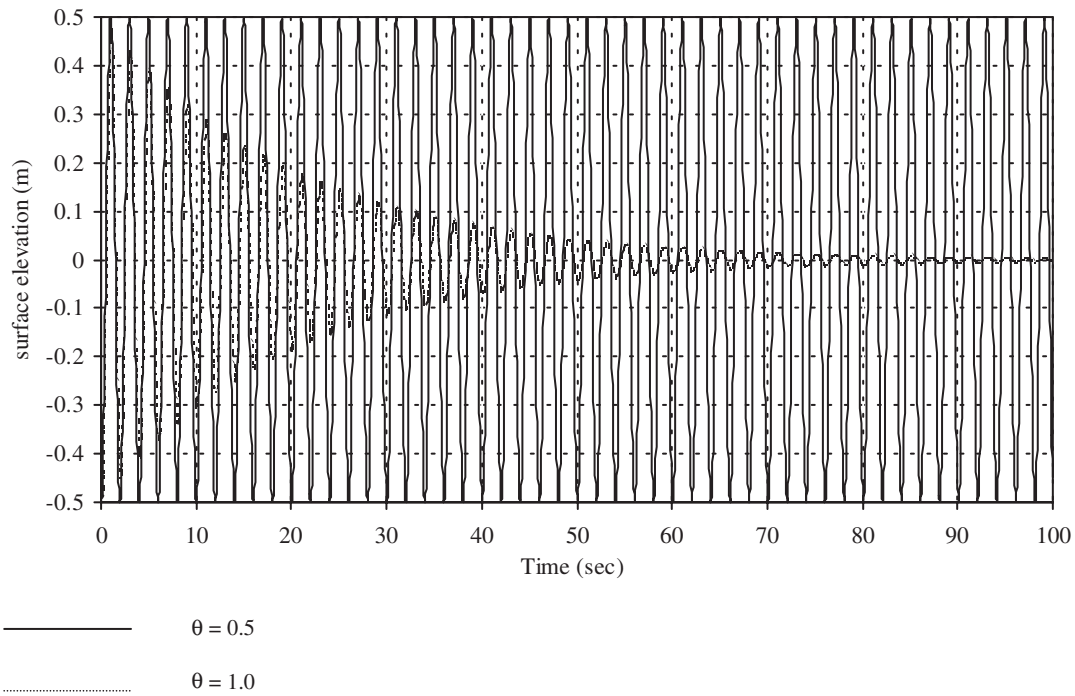

Figure 5. Effect of θ-value on free surface wave damping.

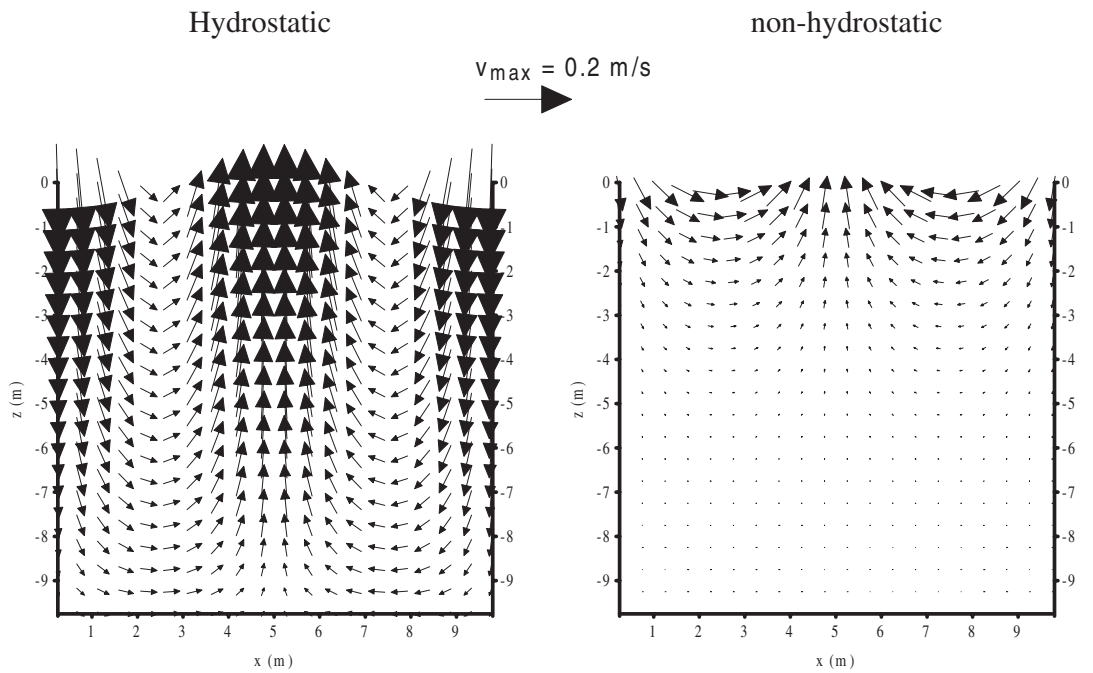

Figure 6. Comparison of hydrostatic and hydrodynamic solutions for small amplitude waves, for same phase angle of $T/4$.

and numerical results. The greatest difference occurs in the pressure field, due to the difference in the boundary conditions at the free surface. In order to demonstrate the behaviour of the numerical solution with and without the hydrostatic pressure assumption after several periods of oscillation, the water surface elevation at $x = 0$ m is plotted in Figure 4, indicating that the wave speed computed without the hydrostatic approximation is in very good agreement with the wave speed estimated analytically for the small amplitude waves. In order to decide what value of θ should be used in the numerical computation, the model was run for about 10 cycles using the fully implicit numerical method with $\theta = 1$ and the semi-implicit method with $\theta = 0.5$, respectively. The numerical results for both θ values are presented in Figure 5, which shows that when a fully implicit numerical method is used the waves are damped slowly and some time later they disappear. For the predictions using the semi-implicit numerical model, the waves are simulated as they should be. Hence, in the model a value of $\theta = 0.5$ is used, leading to a semi-implicit numerical model.

In the second wave test, a more complex wave situation is simulated in the same basin, with $k = 2\pi/nL$ and $n = 4$. The effect of a non-hydrostatic pressure distribution on the flow structure can easily be seen in Figure 6, where both figures were plotted for the same wave phase. For the case of the hydrostatic assumption, the period of the waves is 2.020 s, whereas for the inclusion of the non-hydrostatic pressure the period is 5.062 s. The results shown are at a phase angle of $T/8$, which corresponds to 0.252 and 0.633 s for the cases with and without the hydrostatic assumption, respectively. The difference between the two model

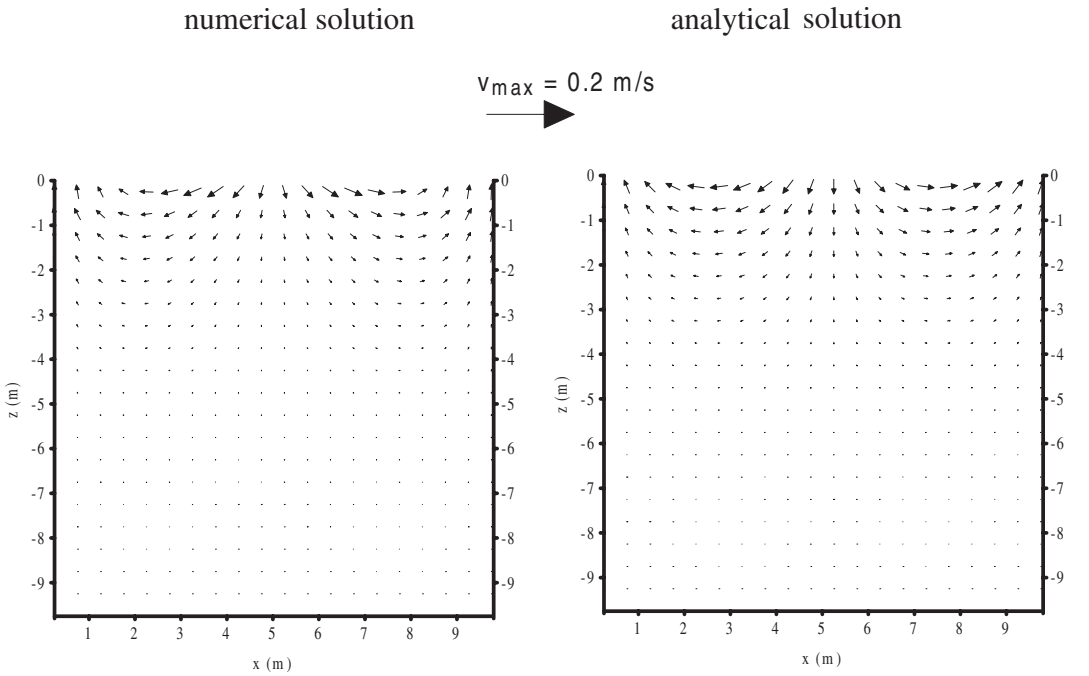

Figure 7. Comparison of numerical and analytical solutions for velocity at $t = 4$ s.

results can clearly be seen. The model with the hydrostatic approximation yields long-wave velocity profiles, which are not realistic and physically not correct, compared to the physically correct and smooth velocity profiles obtained using the non-hydrostatic pressure algorithm. Comparisons of the velocity and hydrodynamic pressure fields in the vertical section are given in Figures 7 and 8 at $t = 4.00$ s ($T/12$), respectively. Again, the agreement between the numerical and analytical results is highly satisfactory and hence it can be concluded that the model simulates the velocity and the hydrodynamic pressure fields correctly.

The other example illustrating the effect of a non-hydrostatic pressure on the velocity field is for a wind-driven circulation in a closed basin. For this classic test case, a basin of length $L = 10$ m, width $W = 1.4$ m and of depth $H = 10$ m is assumed. The wind speed is assumed to be 10 m/s and is blowing in the x-direction. The model includes 20 layers, which are evenly distributed over the depth. The grid spacing in the horizontal plane is 0.2 m, and 0.5 m in the vertical plane. The results of the numerical model with and without the hydrostatic approximation are given in Figure 9. The numerical results with hydrostatic approximation show that there is a strong vertical circulation just near the wall, caused by the evaluation of the vertical velocity component from the continuity equation. The impermeability boundary condition on the wall ensures that there is no flux passing through the wall, setting the horizontal velocity component at the wall to zero. On the other hand, the fluid is accelerated along the fetch path of the wind in the horizontal direction because of the wind stress. This condition builds up a large velocity gradient ($\partial u/\partial x$) near the wall, leading to a large vertical velocity gradient (i.e. $\partial w/\partial z$) due to the continuity equation [6]. Thus, the hydrostatic

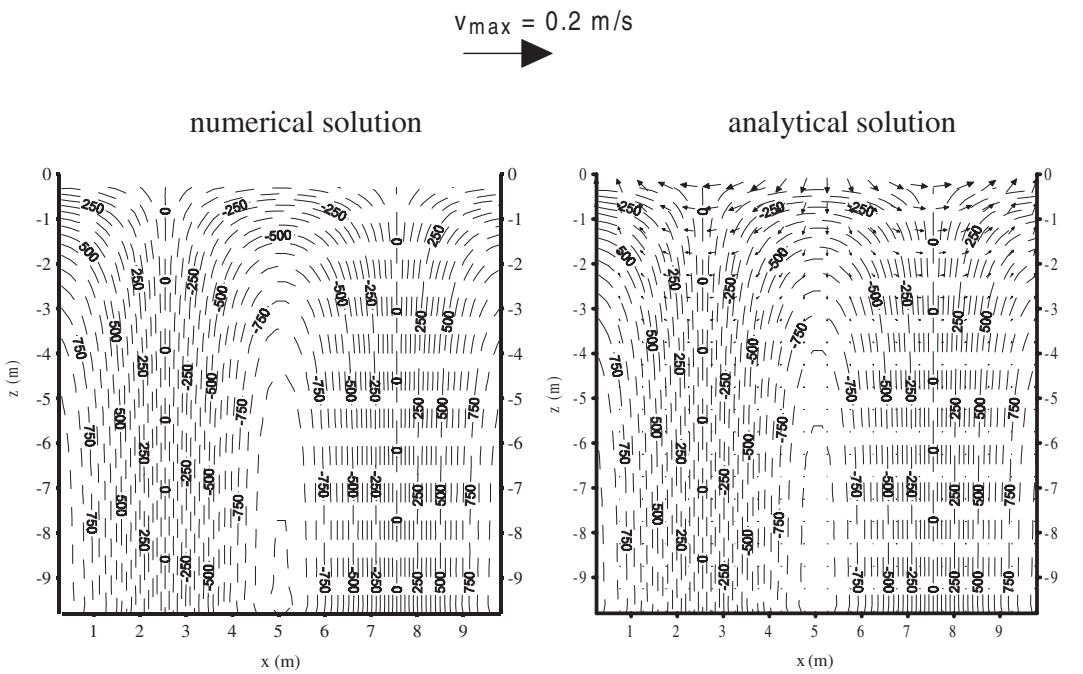

Figure 8. Comparison of numerical and analytical solutions for dynamic pressure at $t = 4$ s.

assumption results in an unrealistic velocity pattern near the wall. Also as clearly seen from the figure there is a strong instability in the flow close to the wall.

The model results obtained using a non-hydrostatic pressure distribution illustrate a smoother horizontal velocity distribution of the vertical flow over the entire section of the basin. With the inclusion of the hydrodynamic pressure gradients, the velocity of the fluid slows down smoothly and the whole vertical circulation pattern is much more realistic.

5. CONCLUSIONS

A three-dimensional numerical model has been developed for predicting free surface flows and with the inclusion of a non-hydrostatic pressure distribution. A semi-implicit finite difference method has been used and a conventional sigma co-ordinate system has been applied in the vertical direction. The hydrostatic and hydrodynamic pressure components are computed in two stages, enabling the model to be run both with and without the hydrostatic pressure assumption. The hydrodynamic pressure is included during the determination of the free surface elevation, so that the effect of the hydrodynamic pressure is included in the solution of the surface elevation. The model has been applied to test cases where hydrodynamic pressure has been shown to have an important effect on the velocity circulation patterns. In all cases the model gives very satisfactory results and highlights the significance of the dynamic pressure term for certain flow fields. The next stage for the authors is to apply the model to an

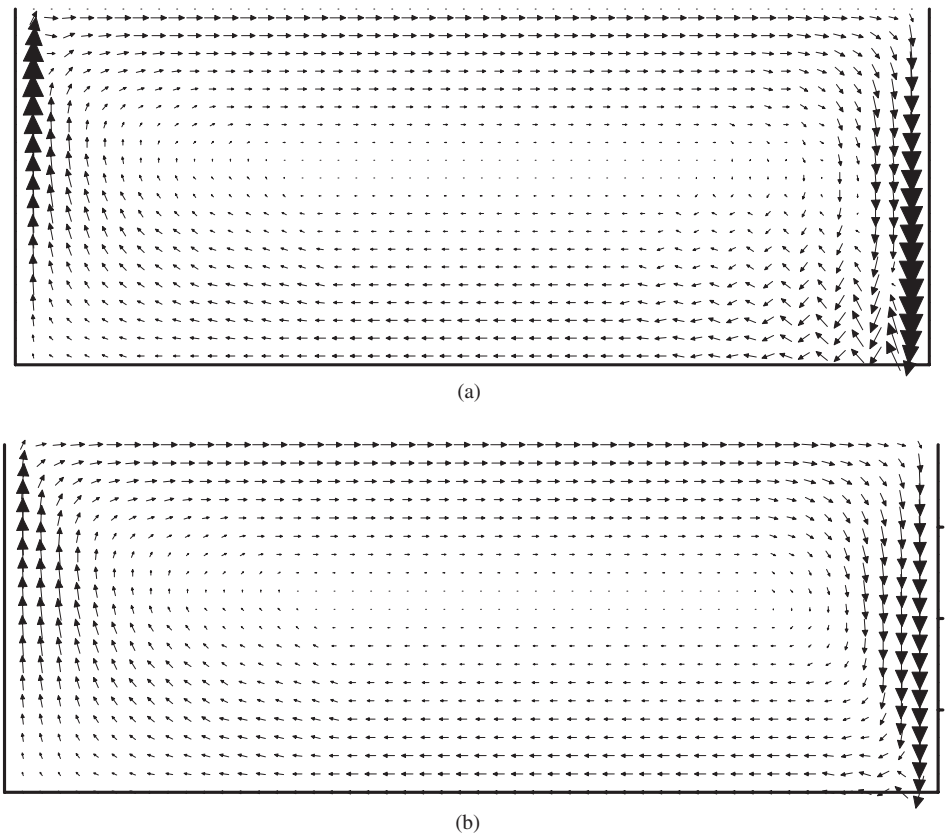

Figure 9. Wind-driven circulation with (a) and without (b) hydrostatic approximation at $T = 2000$ s.

environmental engineering case study, where the vertical acceleration effects can not be neglected, for example to a wind-induced circulation in an inland water body where the bathymetry is complex and having steep slopes.

APPENDIX A

The matrix in x-direction are given as

$$\tilde{\mathbf{U}}^{n+1}_{i+1/2,j} = \begin{bmatrix} \tilde{u}^{n+1}_{i+1/2,j,1} \\ \tilde{u}^{n+1}_{i+1/2,j,2} \\ \vdots \\ \tilde{u}^{n+1}_{i+1/2,j,K} \end{bmatrix}, \quad \mathbf{G}^{n}_{i+1/2,j} = \begin{bmatrix} Fu^{n}_{i+1/2,j,1} + \Delta t \tau^{\mathrm{w}}_{x} \\ Fu^{n}_{i+1/2,j,2} \\ \vdots \\ Fu^{n}_{i+1/2,j,K} \end{bmatrix}, \quad \boldsymbol{\Delta}\sigma^{n}_{i+1/2,j} = \begin{bmatrix} \Delta\sigma^{n}_{i+1/2,j,1} \\ \Delta\sigma^{n}_{i+1/2,j,2} \\ \vdots \\ \Delta\sigma^{n}_{i+1/2,j,K} \end{bmatrix}$$

$$A^n_{i+1/2,j} = \begin{vmatrix} \Delta\sigma^n_{i+1/2,j,k} + \Delta t \frac{v_{i+1/2,j,k+1/2}}{\Delta\sigma^n_{i+1/2,j,k+1/2}} & \Delta t \frac{v_{i+1/2,j,k+1/2}}{\Delta\sigma^n_{i+1/2,j,k+1/2}} & & 0 \\ -\Delta t \frac{v_{i+1/2,j,k-1/2}}{\Delta\sigma^n_{i+1/2,j,k-1/2}} & \Delta\sigma^n_{i+1/2,j,k} + \Delta t \frac{v_{i+1/2,j,k+1/2}}{\Delta\sigma^n_{i+1/2,j,k+1/2}} & \Delta t \frac{v_{i+1/2,j,k+1/2}}{\Delta\sigma^n_{i+1/2,j,k+1/2}} & \\ \vdots & \vdots & \vdots & \vdots \\ 0 & & -\Delta t \frac{v_{i+1/2,j,K-1/2}}{\Delta\sigma^n_{i+1/2,j,K-1/2}} & \Delta\sigma^n_{i+1/2,j,K} + \Delta t \frac{v_{i+1/2,j,K+1/2}}{\Delta\sigma^n_{i+1/2,j,K+1/2}} + \Delta t\gamma \end{vmatrix}$$

where γ is related to the bed stress and defined as

$$\gamma = \frac{\sqrt{(u^n_{i+1/2,j,K})^2 + (v^n_{i,j+1/2,K})^2}}{\left[2.5 \ln\left(\frac{30d}{2.72k_s}\right)\right]^2}$$

ACKNOWLEDGEMENTS

The research grant provided for the first author by Turkish Government is greatly acknowledged.

REFERENCES

1. Stansby PK, Zhou JG. Shallow water flow solver with non-hydrostatic pressure: 2D vertical plane problems. *International Journal for Numerical Methods in Fluids* 1998; **28**:541–563.
2. Zhou JG, Stansby PK. An arbitrary Langrangian–Eulerian sigma (ALES) model with non-hydrostatic pressure for shallow water flows. *Computational Methods in Applied Mechanical Engineering* 1999; **178**:199–214.
3. Li Z, Johns B. A numerical method for the determination of weakly non-hydrostatic non-linear free surface wave propagation. *International Journal for Numerical Methods in Fluids* 2001; **35**:2997–3317.
4. Gaarthuis J. A non-hydrostatic pressure model for shallow water flow: analysis and application of three methods to compute a non-hydrostatic correction term. *Ph.D. Thesis*, Technische Universiteit, Eindhoven, 1995.
5. Casulli V, Stelling GS. Numerical simulation of three dimensional, quasi-hydrostatic free-surface flows. *Journal of Hydraulic Engineering, ASCE* 1998; **124**(7):678–686.
6. Jankowski JA. A non-hydrostatic model for free surface flows. *Ph.D. Thesis*, Hannover University, Germany, 1999.
7. Rodi W. *Turbulence models and their applications in Hydraulics* (2nd edn). IAHR Publication: Delft, 1984.
8. Haney RL. On the pressure gradient force over steep topography in sigma co-ordinate ocean models. *AMS Journal of Physical Oceanography* 1991; **21**(4):610–619.
9. Stelling G, van Kester JATM. On the approximation of horizontal gradients in sigma co-ordinates for bathymetry with steep bottom slopes. *International Journal for Numerical Methods in Fluids* 1994; **18**:915–935.

